

NANO EXPRESS

Open Access



Structural and Visible-Near Infrared Optical Properties of Cr-Doped TiO₂ for Colored Cool Pigments

Le Yuan^{1,2}, Xiaolong Weng^{1*}, Ming Zhou², Qingyong Zhang² and Longjiang Deng¹

Abstract

Chromium-doped TiO₂ pigments were synthesized via a solid-state reaction method and studied with X-ray diffraction, SEM, XPS, and UV-VIS-NIR reflectance spectroscopy. The incorporation of Cr³⁺ accelerates the transition from the anatase phase to the rutile phase and compresses the crystal lattice. Moreover, the particle morphology, energy gap, and reflectance spectrum of Cr-doped TiO₂ pigments is affected by the crystal structure and doping concentration. For the rutile samples, some of the Cr³⁺ ions are oxidized to Cr⁴⁺ after sintering at a high temperature, which leads to a strong near-infrared absorption band due to the ³A₂ → ³T₁ electric dipole-allowed transitions of Cr⁴⁺. And the decrease of the band gap causes an obvious redshift of the optical absorption edges as the doping concentration increases. Thus, the VIS and near-infrared average reflectance of the rutile Ti_{1-x}Cr_xO₂ sample decrease by 60.2 and 58%, respectively, when the Cr content increases to x = 0.0375. Meanwhile, the color changes to black brown. However, for the anatase Ti_{1-x}Cr_xO₂ pigments, only the VIS reflection spectrum is inhibited by forming some characteristic visible light absorption peaks of Cr³⁺. The morphology, band gap, and NIR reflectance are not significantly affected. Finally, a Cr-doped anatase TiO₂ pigment with a brownish-yellow color and 90% near-infrared reflectance can be obtained.

Keywords: Titanium dioxide, Cr-doping, Reflection spectrum, Color, Cool pigment

Background

TiO₂ is an important cool pigment applied widely in energy-efficient buildings due to its high visible light (VIS) and near-infrared (NIR) reflectance (> 85%) [1, 2]. Since the sunlight in visible light and near-infrared waveband plays the most important role in heat generation [3, 4], heat-reflective paints prepared by TiO₂ pigments can obviously decrease the heat accumulation of buildings. This results in a decrease of more than 20% in energy consumption for air conditioning [4]. However, because of the high VIS reflectance of TiO₂ pigment, the resulting white paint is very bright and unpleasant to the human eye. This also leads to poor esthetics, low stain resistance, and a short lifespan [5, 6]. To overcome these limitations, numerous efforts have been made to develop

a novel non-white cool pigment with low lightness and low VIS reflectance while retaining the high NIR reflectance. However, it is difficult to appropriately control the VIS and NIR reflection spectrum simultaneously.

Elemental doping is an effective VIS spectral controlling method that is widely used in many fields, including photo catalysis, photoluminescence, and ceramic pigments [7–9]. For oxide pigment, the doped ions are helpful in forming impurity levels, reducing the band gap, and increasing the ability to absorb low-energy photons, such as the diffuse reflectance spectra of the doped TiO₂ that can be significantly shifted to longer wavelengths with enhanced visible absorption [10–12]. Hence, it can be used to prepare various colored pigments, such as orange (doping Cr element), tan (Mn), yellow (Ni), and gray (V) [9, 10].

In addition to enhancing the visible light absorption, doped ions further influence the concentrations of the free carriers. Because free carrier absorption is the main photon absorption mechanism in the NIR region, the

* Correspondence: wengxl59@163.com

¹National Engineering Research Center of Electromagnetic Radiation Control Materials, University of Electronic Science and Technology of China, Chengdu 610054, People's Republic of China

Full list of author information is available at the end of the article

NIR reflectance of oxide pigments can be improved by controlling the concentrations of free carriers. In addition, the NIR reflectance is also connected to the TiO₂ host material properties, such as crystal structure, particle morphology, and size. In view of the different mechanisms influencing VIS and NIR reflectance, doped TiO₂ pigments should be able to be prepared with dark color and high NIR reflectance. This would simultaneously satisfy the need for energy savings and a pleasing color palette.

The aim of this work is to explore the applicability of Cr-doped TiO₂ as a colored cool pigment. Several samples with different Cr-doped concentrations and sintering temperatures were synthesized via a solid-state reaction method. The influences on crystalline phase, morphology, chemical components, color, and the VIS-NIR reflection spectrum were systematically investigated.

Experimental

Synthesis of Ti_{1-x}Cr_xO₂ Pigment

In a typical solid-state reaction process of Ti_{1-x}Cr_xO₂ samples, stoichiometric commercial-grade raw materials of TiO₂ (99.9%) and Cr₂O₃ (99.9%) were milled using a planetary ball mill for 4 h at 450 rpm in ethanol. Agate jar and balls were used. The weight of the mixed powder sample was 50 g, and the ratio of ball weight to sample weight was 10:1. Residual ethanol was removed by evaporation drying about 80 °C. The grinded powders were then calcined at temperature of 800–1000 °C for 4 h in air atmosphere at the heating rate of 5 °C/min. The ensuing pigment powders were ground in agate mortar.

Characterization

The samples were characterized by X-ray diffraction (D2 PHASER with CuKα radiation, Bruker) and field emission scanning electron microscopy (QUANTA 250, FEI). The lattice constants were calculated from the XRD patterns using the MDI Jade software package. X-ray photoelectron spectroscopy with Al Kα X-ray ($h\nu = 1486.6$ eV) radiation operated at 150 W (Thermo Scientific Escalab 250Xi, USA) was used to investigate the surface properties. The shift of the binding energy due to the relative surface charging was corrected using the C 1s level at 284.8 eV as an internal standard. The UV-VIS-NIR reflection spectrum (250–2500 nm) was measured with a UV-VIS-NIR spectrophotometer (Lambda 750, Perkin-Elmer). The CIE LAB color data (L^* , a^* , and b^*) were calculated from the visible light reflection spectrum by Color CIE software (Perkin-Elmer, CIE D65 photo source, and 10° observation angle; the calculated spectrum range was 400–700 nm). And the band gap E_g of powder samples was extracted via the following equation [13, 14]:

$$\begin{cases} [F(R)h\nu]^2 = C(h\nu - E_g) \\ F(R) = \frac{(1-R)^2}{2R} \end{cases} \quad (1)$$

where $F(R)$ is the Kubelka-Munk function, R is the diffuse reflectance, $h\nu$ is the photon energy, and C is the proportionality constant.

Result and Discussion

Phase Structure of the Samples

The XRD patterns of Ti_{1-x}Cr_xO₂ powders with various Cr-doped concentrations obtained at different sintering temperatures from 800 °C to 1000 °C are shown in Fig. 1. The samples calcined at 800 °C have only diffraction peaks of the anatase phase (JCPDS, File No. 21-1272). Traces of the diffraction peaks of the rutile phase (JCPDS, File No. 21-1276) can be found until the doping concentration reaches $x = 0.0375$.

When the sintering temperature is 900 °C (Fig. 1b), the undoped TiO₂ sample ($x = 0$) has only an anatase crystal structure. It began to transform to the rutile phase as the Cr³⁺ ions are doped into the TiO₂ matrix. Furthermore, the rutile phase continuously increases with the increasing Cr³⁺ concentration. With the continued increase in sintering temperature to 1000 °C (XRD data; Fig. 1c), there are both the anatase and rutile phases of TiO₂ in the undoped product. However, the anatase peaks are not detected in Ti_{1-x}Cr_xO₂ products. This illustrates that the Cr³⁺ ions accelerate the crystal phase transformation from anatase to rutile and the phase transition temperature can be reduced by around 100 °C. This is because when the valence (III) cations diffuse in the titania lattice, they provide a charge compensation process to form oxygen vacancies that enhance the transport of atoms and accelerate the anatase-to-rutile phase transition [15, 16].

The Ti_{1-x}Cr_xO₂ products calcined at 800 ~ 1000 °C have no chromium oxide diffraction peaks in XRD, which indicates that the Cr dopants are well-dispersed on the TiO₂ matrix. In addition, the lattice constant of the Ti_{1-x}Cr_xO₂ products is also affected by the concentration of Cr³⁺ impurities (Table 1). Although Cr³⁺ has a slightly larger size (75.5 pm) than Ti⁴⁺ (74.5 pm), the lattice constant of Ti_{1-x}Cr_xO₂ products decreases with increasing Cr³⁺ concentration regardless of anatase or rutile structure. This might be because of the oxygen vacancy that is formed when Ti–O breaks and Cr³⁺ substitutes into the Ti⁴⁺ lattice sites [17]. Higher Cr³⁺ concentrations result in more oxygen vacancies. An oxygen deficiency could diminish the number of Ti–O or Cr–O bonds, and this leads to contraction of the O–Ti–O or O–Cr–O bond angle [17]. On the other hand, some Cr³⁺ is

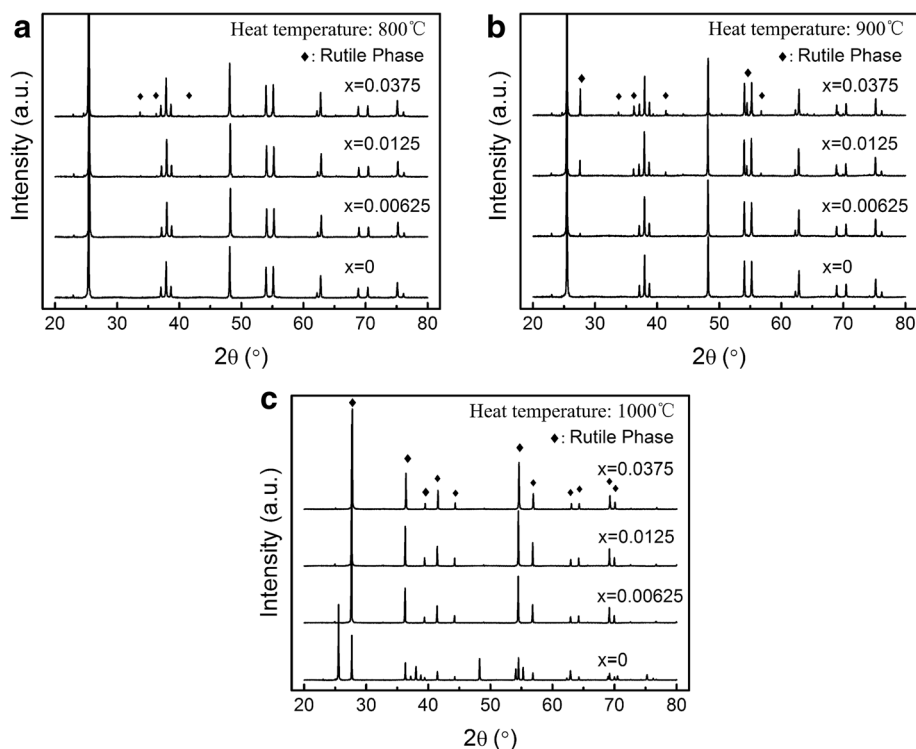


Fig. 1 a–c XRD patterns of $\text{Ti}_{1-x}\text{Cr}_x\text{O}_2$ products prepared at different sintering temperatures and doping concentrations (Sintering temperature is a: 800°C; b: 900°C; c: 1000°C)

gradually oxidized to the smaller Cr^{4+} (55 pm) during the high-temperature sintering process. The overall result is a squeezing of the lattice and a reduction in the values of the lattice constant.

Sample Morphology

Figure 2 shows SEM images of undoped TiO_2 and $\text{Ti}_{1-x}\text{Cr}_x\text{O}_2$ products prepared at different sintering temperatures and Cr concentrations. The morphology of undoped TiO_2 samples sintered at 800 °C are nearly spherical, and the average particle size is less than 100 nm. The morphology and particle size have no obvious change upon doping low concentrations of Cr^{3+} ($x = 0.00625$). However, if the doping concentration of Cr^{3+} is too high ($x = 0.0375$), then the particle size

would slightly increase, and the morphology becomes non-uniform.

When the temperature increases to 1000 °C, nearly spherical and nearly cubic particles are observed simultaneously in the undoped samples (Fig. 2d) due to the coexistence of anatase and rutile structures. The particle morphology changes to the elongated columnar shape after the Cr^{3+} dopant is added. However, the aspect ratio decreases, and particle size increases with increasing dopant content. There is a tendency to return to a spherical particle again at high doping concentrations. As the doping amount increases to $x = 0.0375$ relative to the undoped sample, the average particle size increases from 300 nm to 2 μm .

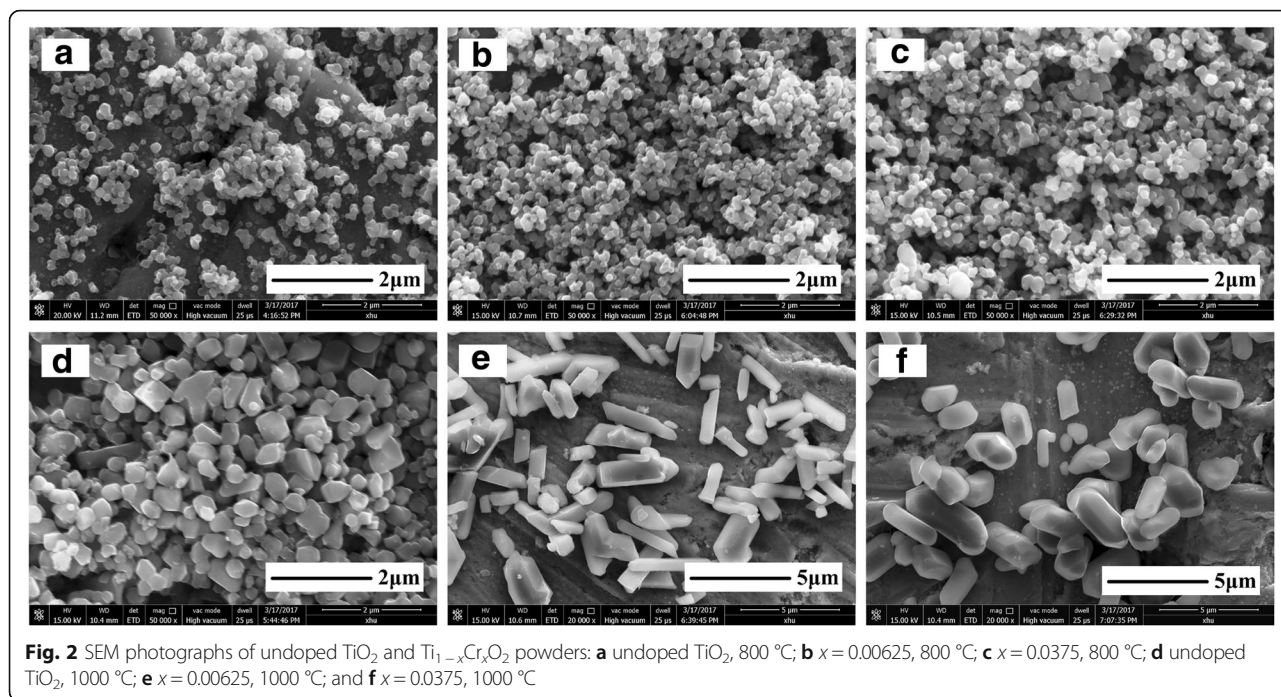
XPS Analysis

The XPS spectrum of Cr-doped TiO_2 powders reveals Cr, Ti, and O. The Ti 2p XPS spectra are presented in Fig. 3a. The results show that there are two major peaks located near 458.9 to 458.3 eV and 464.2 to 464.1 eV. The locations of the major peaks represent the Ti 2p_{1/2} and Ti 2p_{3/2} orbit, respectively, indicating that the Ti element mainly exists as a chemical state of Ti^{4+} [11].

Figure 3-b indicates that all of the samples have two pronounced Cr-2p XPS peaks with binding energies of 577 eV and 586.4 eV, which are consistent with the values of Cr^{3+} in the TiO_2 lattices [18]. The other peaks

Table 1 Variation in the lattice constant with Cr concentrations

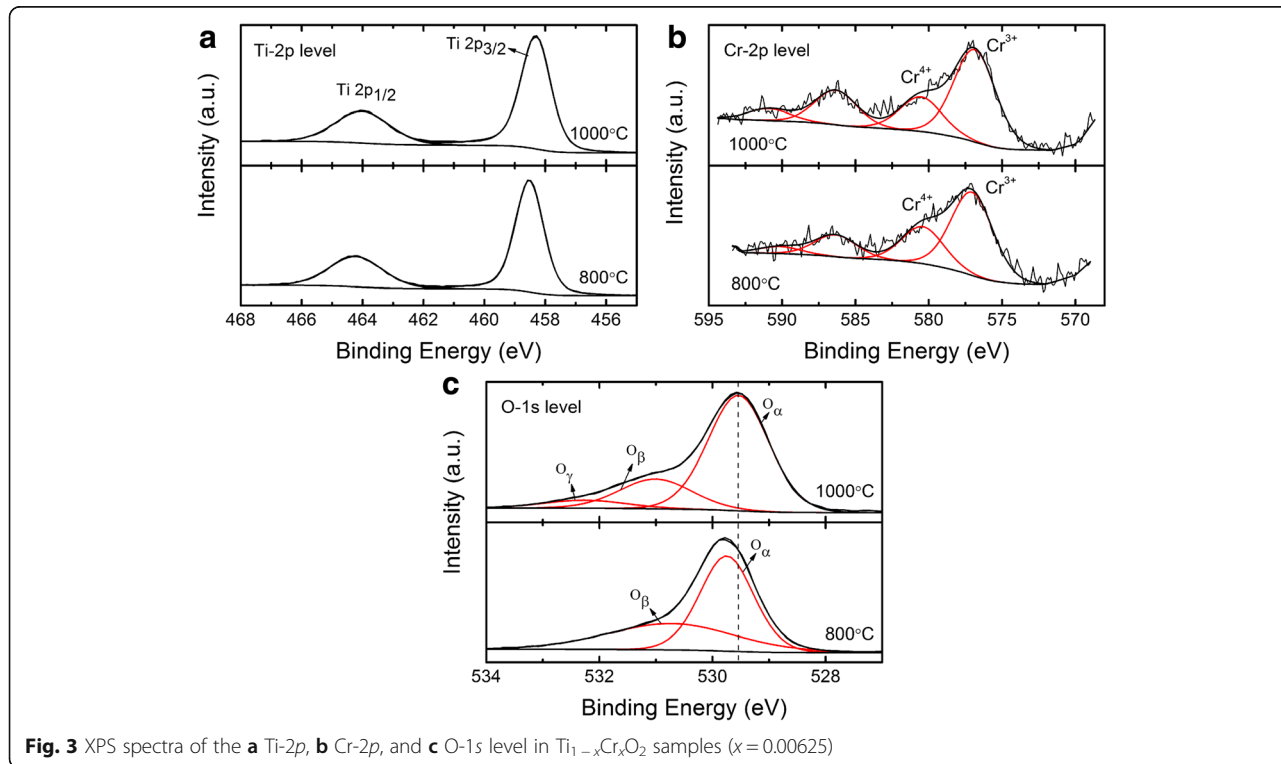
The impurity concentration	Lattice constant					
	800 °C (anatase)			1000 °C (rutile)		
	$a = b$ (Å)	c (Å)	Vol (Å ³)	$a = b$ (Å)	c (Å)	Vol (Å ³)
$x = 0$	3.778	9.499	135.56	–	–	–
$x = 0.00625$	3.771	9.486	134.89	4.575	2.952	61.79
$x = 0.0125$	3.769	9.483	134.74	4.573	2.952	61.73
$x = 0.025$	3.768	9.480	134.56	4.571	2.948	61.6
$x = 0.0375$	3.767	9.476	134.47	4.566	2.946	61.41



are located at 580.6 eV and 591 eV, and these are attributed to Cr^{4+} ions [18]. Meanwhile, the area ratios of the Cr^{4+} peak at 580.6 eV increases from 29.6% to 35.8% with annealing temperatures that increase from 800 °C to 1000 °C. Tetravalent Cr^{4+} has been reported to form via a charge compensation reaction triggered by evaporation of

Cr [18]. The relative content of Cr^{4+} increases as the annealing temperature increases because the evaporation could be enhanced at a high temperature.

The XPS spectra of O 1s are shown in Fig. 3c. For the sample sintered at 800 °C, the O 1s peaks comprise two overlapping peaks, indicating the existence of different



types of oxygen on the samples' surface. The lower binding energy peak at 529.8 eV is attributed to the lattice oxygen (O_a) [19]. The other overlapping peak at a binding energy of 530.8 is attributed to surface adsorbed oxygen (O_b). Specifically, a new overlapping peak is formed at 532.3 eV due to the surface oxygen of hydroxyl or absorbed water (O_v) as the annealing temperature increased from 800 to 1000 °C [19]. Moreover, the binding energy of the O 1s peaks tends to shift slightly towards a lower binding energy (approximately 0.2 eV) with an increasing annealing temperature. This redshift is consistent with the conversion of Cr^{3+} into Cr^{4+} [20, 21].

The Optical Property of the Samples

Figure 4 shows the colorimetric values of $Ti_{1-x}Cr_xO_2$ pigments with different sintering temperatures and doping concentrations. For the samples obtained at 800 °C, the variation in luminosity (L^*) is negligible as the dopant content increased. Meanwhile, the red component (a^*) and yellow component (b^*) first increase and then

decrease with the increasing concentration of the Cr^{3+} impurity. Thus, the color of as-prepared anatase pigments changed from the original white into a brownish-yellow color.

When the sintering temperature increases to 1000 °C, the variations in L^* and b^* are more pronounced. As the Cr dopant content increases from $x=0$ to 0.0375, the value of L^* and b^* decreases by 43.9 and 1.9, respectively. However, the change in a^* is not the same as that of anatase samples that increase monotonously with the increasing Cr concentration. In the rutile $Ti_{1-x}Cr_xO_2$ pigments, the color changed remarkably from pale yellow to black brown, and the visible brightness was significantly inhibited. Thus, the Cr dopant can effectively modulate the color of rutile pigments, but there is little change on the anatase samples. The differential impact of Cr-doping on color properties is caused by the differences in the visible light reflectance spectrum. A lower visible reflectance results in more absorbed photons and a deeper color.

Figure 5 shows the UV-VIS-NIR diffuse reflectance spectra of undoped TiO_2 and $Ti_{1-x}Cr_xO_2$ products with different sintering temperatures and Cr concentrations. Figure 6 shows the average spectral reflectivity of samples in the VIS (0.4–0.8 μm) and NIR (0.8–2.5 μm) ranges, respectively. The absorption peaks at 1384, 1926, and 2210 nm are attributable to the testing equipment and fixture in the spectra curves. Figures 5 and 6 show that the undoped TiO_2 samples, whether anatase or rutile, have extremely high spectral reflectance in their near-infrared waveband ($\sim 90\%$). As the crystal phase transitions from anatase to rutile, its visible reflectance is still more than 80% even though the VIS absorption increased slightly.

For the Cr-doped anatase TiO_2 sample, some extra absorption peaks can be detected in the visible light reflection curve. The VIS absorption peak at ~ 710 nm is related to the d-d electronic transition of Cr^{3+} in the octahedral crystal field of TiO_2 [22], which could be assigned to the ${}^4A_2(F) \rightarrow {}^2E$ electronic spin allowed transitions of Cr^{3+} [17]. At higher Cr^{3+} concentrations, there is stronger intensity absorption in the VIS waveband. Thus, the average VIS reflectance declines from 90.3% ($x=0$) to 68.2% ($x=0.0375$). Although the VIS reflectivity spectra are somewhat inhibited, the samples can maintain high reflectance in the near-infrared waveband ($\sim 90\%$).

When the sintering temperature increases to 1000 °C, the rutile phase TiO_2 are finally transformed by anatase phase TiO_2 in the Cr-doped products according to the XRD data. Figure 5c indicates two new absorption shoulders located at 450 and 600 nm in the rutile TiO_2 samples. In particular, a strong and broad absorption band appeared in the near-infrared spectrum (about

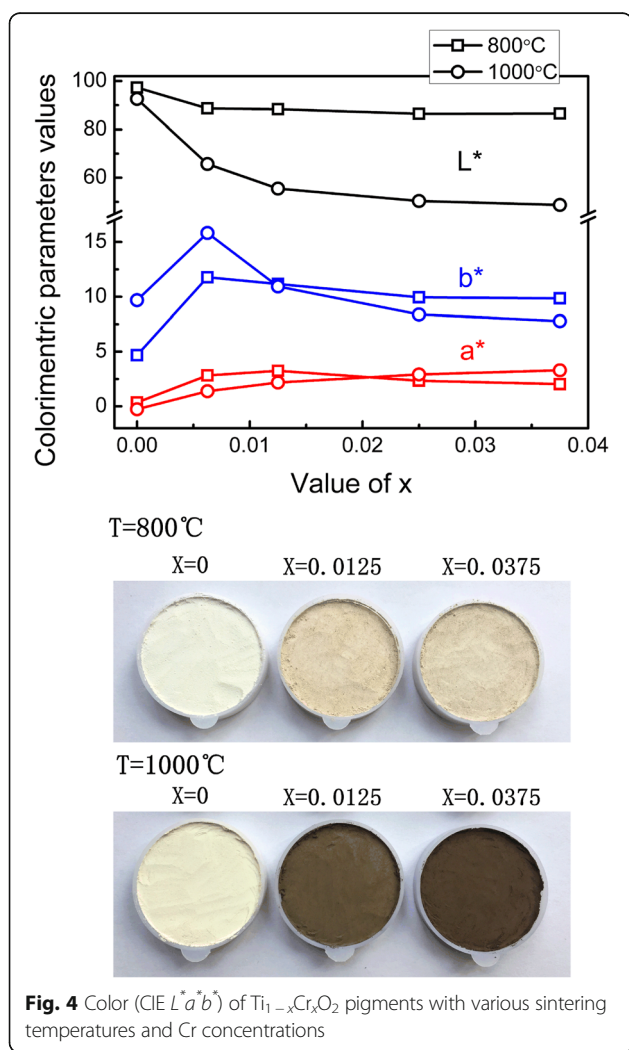
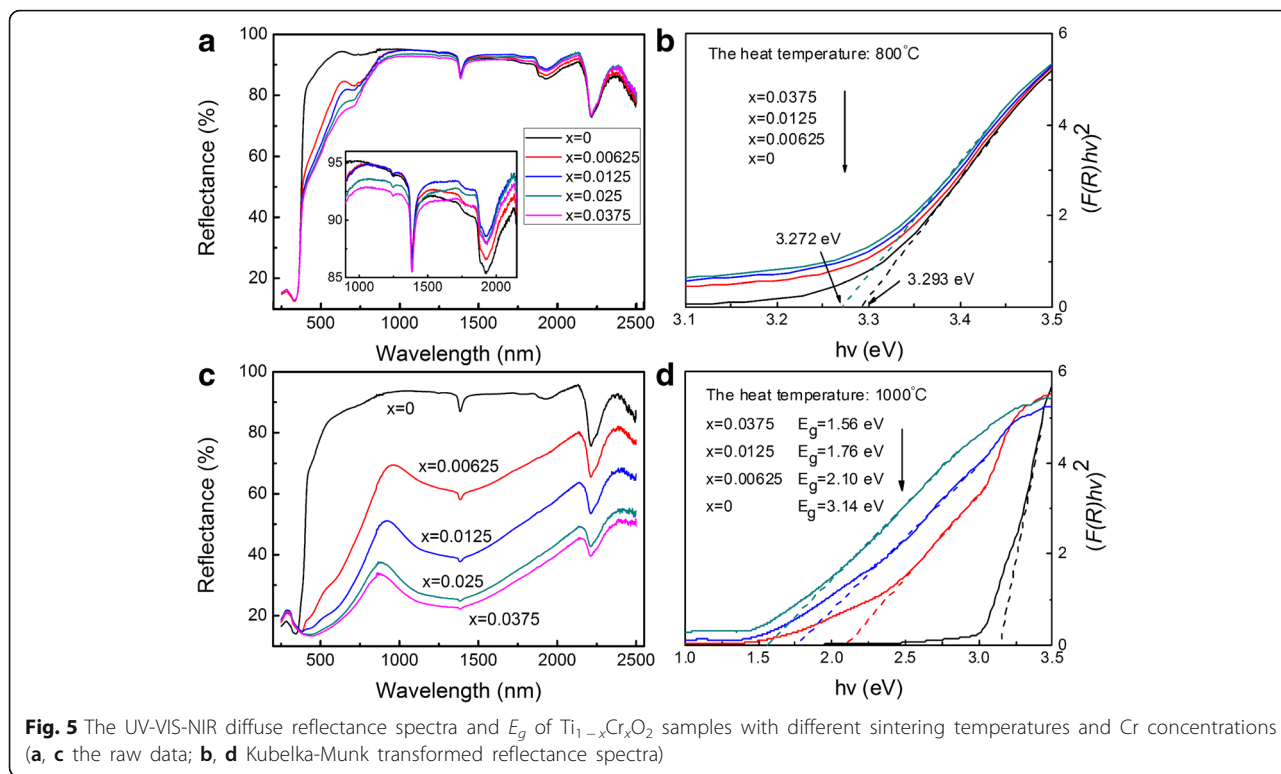


Fig. 4 Color (CIE $L^*a^*b^*$) of $Ti_{1-x}Cr_xO_2$ pigments with various sintering temperatures and Cr concentrations

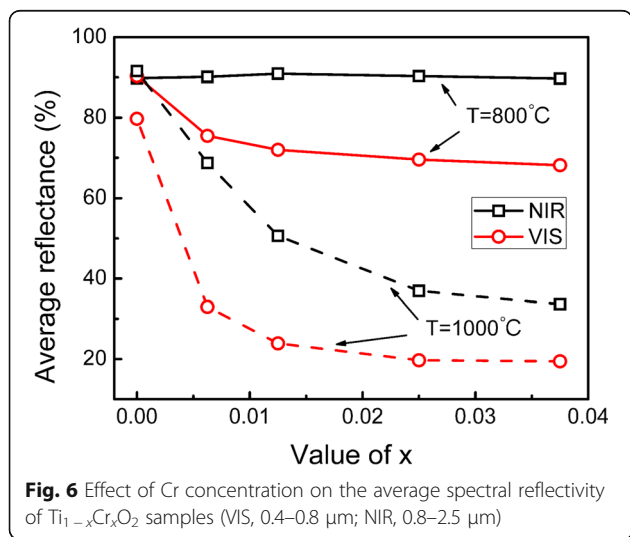


1150 ~ 1500 nm). This is attributed to the $^3A_2 \rightarrow ^3T_1$ electric dipole-allowed transitions of Cr^{4+} in the tetrahedral coordination [23, 24]. The absorption intensity gradually enhances with increasing dopant concentration.

In addition, the absorption edge of the rutile $Ti_{1-x}Cr_xO_2$ samples has an obvious redshift. However, there is no significant change in the absorption edge of the anatase samples. The diffuse reflectance spectra of the samples after Kubelka-Munk treatment are shown in Fig. 5b, d. The intersection between the linear fit and the photon energy axis gives the value to E_g . The

relationship of band gap energy with absorption edge ($E_g = 1240/\lambda_g$) suggests that the redshift of the absorption edge indicates a decrease in the band gap. Figure 5b shows that the doping process would not significantly alter the value of E_g for the anatase samples. This adds only 0.021 eV with the Cr content that increases to $x = 0.0375$. In contrast, the E_g value of rutile $Ti_{1-x}Cr_xO_2$ samples dropped sharply with the increasing doping concentration. The band gap reduces to 1.56 eV when the doping concentration is $x = 0.0375$.

In conclusion, the influence of Cr dopants on the spectral characteristic of TiO_2 depends significantly on the crystal structure of the host materials. After introducing Cr dopant into the anatase TiO_2 sample, only some characteristic absorption peaks appear in the visible light waveband due to the formation of an impurity energy level, while the band gap and NIR reflectance are not significantly affected. Thus, the near-infrared reflectance of anatase $Ti_{1-x}Cr_xO_2$ pigments remains at 90%. In rutile TiO_2 , however, the doping process leads to strong characteristic absorption peaks in both the VIS and NIR region. In addition, the decrease in band gap, E_g , results in the enhanced capability to absorb lower energy photons. The VIS and NIR average reflectance of the rutile $Ti_{1-x}Cr_xO_2$ sample decreases by 60.2 and 58%, respectively, as the Cr content increases from $x = 0$ to 0.0375.



Conclusions

We conclude that the crystalline phase, morphology, and optical properties of $\text{Ti}_{1-x}\text{Cr}_x\text{O}_2$ pigments are obviously affected by the sintering temperature and Cr-doped concentration. The incorporation of Cr^{3+} can accelerate the transition from anatase phase to rutile phase and compress the crystal lattice resulting in a 100 °C decrease in phase transition temperature. The doped ions rarely affect the morphology of anatase samples, but greatly increase the particle size and morphology of the rutile samples. This changes the morphology of rutile particles from columnar to near spherical at high doping concentrations.

Furthermore, the doping ions and crystalline structure have an important influence on the energy gap and optical properties of $\text{Ti}_{1-x}\text{Cr}_x\text{O}_2$ pigments. Cr^{3+} is gradually oxidized to Cr^{4+} during high-temperature sintering, and the Cr^{4+} content is greater as the sintering temperature increases. The generated Cr^{4+} ions lead to a strong NIR absorption band for rutile samples due to the ${}^3\text{A}_2 \rightarrow {}^3\text{T}_1$ electric dipole-allowed transitions of Cr^{4+} . Furthermore, the band gap values of the rutile samples decreased gradually, and its absorption edges exhibited an obvious redshift as the doping concentration increased. This greatly enhanced the capability to absorb lower energy photons. Thus, the visible color changes to black brown as the Cr content increases from $x = 0$ to 0.0375. The VIS and NIR average reflectance of the rutile $\text{Ti}_{1-x}\text{Cr}_x\text{O}_2$ sample decreases by 60.2 and 58%, respectively.

Conversely, the anatase samples have only some characteristic absorption peaks that appear in the VIS waveband due to the formation of the impurity energy level of Cr^{3+} . However, the band gap and NIR reflectance are not significantly affected. Thus, Cr-doped anatase TiO_2 pigment with a brownish-yellow color and 90% near-infrared reflectance were obtained through this process.

Abbreviations

a^* : the CIE red component; b^* : the CIE yellow component; L^* : the CIE luminosity; NIR: Near infrared; UV: Ultraviolet; VIS: Visible light

Acknowledgements

Not applicable.

Authors' Contributions

LY prepared the Cr-doped TiO_2 samples and writing of the manuscript. XLW conceived of this study. MZ measured the reflectance spectrum and analyzed the optical property. QYZ analyzed the XRD and XPS data. LJD carried out the manuscript modification. All authors read and approved the final manuscript.

Funding

This work presented in this paper was supported by the National Natural Science Foundation of China (No. 51402241), the Research Project of the Education Department of Sichuan Province (No. 15ZB0138), and the Open Research Subject of Key Laboratory of Special Materials and Manufacturing Technology (No. SZJJ2017-063).

Competing Interests

The authors declare that they have no competing interests.

Publisher's Note

Springer Nature remains neutral with regard to jurisdictional claims in published maps and institutional affiliations.

Author details

¹National Engineering Research Center of Electromagnetic Radiation Control Materials, University of Electronic Science and Technology of China, Chengdu 610054, People's Republic of China. ²Key Laboratory of Fluid and Power Machinery of Ministry of Education, Center for Advanced Materials and Energy, Xihua University, Chengdu 610039, People's Republic of China.

Received: 11 October 2017 Accepted: 6 November 2017

Published online: 17 November 2017

References

- Zhou YX, Weng XL, Yuan L, Deng LJ (2014) Influence of composition on near infrared reflectance properties of M-doped Cr_2O_3 (M=Ti, V) green pigments. *J Ceram Soc Jpn* 122:311–316
- Thongkanluang T, Limsuwan P, Rakkwamsuk P (2011) Preparation and application of high near-infrared reflective green pigment for ceramic tile roofs. *Int J Appl Ceram Tec* 8:1451–1458
- Oka R, Masui T (2016) Synthesis and characterization of black pigments based on calcium manganese oxides for high near-infrared (NIR) reflectance. *RSC Adv* 6:90952–90957
- Levinson R, Berdahl P, Akbari H (2005) Solar spectral optical properties of pigments—part I: model for deriving scattering and absorption coefficients from transmittance and reflectance measurements. *Sol Energy Mat Sol C* 89:319–349
- Baneshi M, Maruyama S, Komiya A (2012) The effects of TiO_2 pigmented coatings characteristics on temperature and brightness of a coated black substrate. *Sol Energy* 86:200–207
- Levinson R, Akbari H, Berdahl P, Wood K, Skilton W, Petersheim J (2010) A novel technique for the production of cool colored concrete tile and asphalt shingle roofing products. *Sol Energy Mat Sol C* 94:946–954
- Tse MY, Tsang MK, Wong YT, Chan YL, Hao J (2016) Simultaneous observation of up/down conversion photoluminescence and colossal permittivity properties in (Er+Nb) co-doped TiO_2 materials. *Appl Phys Lett* 109:139
- Sreeram KJ, Aby CP, Nair BU, Ramasami T (2008) Colored cool colorants based on rare earth metal ions. *Sol Energy Mat Sol C* 92:1462–1467
- Dondi M, Cruciani G, Guarini G, Matteucci F, Raimondo M (2006) The role of counterions (Mo, Nb, Sb, W) in Cr-, Mn-, Ni- and V-doped rutile ceramic pigments: part 2. Colour and technological properties. *Ceram Int* 32:393–405
- Zou J, Zhang P, Liu C, Peng Y (2014) Highly dispersed (Cr, Sb)-co-doped rutile pigments of cool color with high near-infrared reflectance. *Dyes Pigments* 109:113–119
- Liu Z, Xing L, Ma H, Cheng L, Liu J, Yang J, Zhang Q (2016) Sulfated Ce-doped TiO_2 as visible light driven photocatalyst: preparation, characterization and promotion effects of Ce doping and sulfation on catalyst performance. *Environ Prog Sustain* 36:494–454
- Ansari SA, Khan MM, Ansari MO, Cho MH (2016) Nitrogen-doped titanium dioxide (N-doped TiO_2) for visible light photocatalysis. *New J Chem* 40: 3000–3009
- Morales AE, Mora ES, Pal U (2007) Use of diffuse reflectance spectroscopy for optical characterization of un-supported nanostructures. *Rev Mex Fis* 53: 18–22
- Zachary MG, Aaron L, Snyder GJ (2013) Optical band gap and the Burstein–Moss effect in iodine doped PbTe using diffuse reflectance infrared Fourier transform spectroscopy. *New J Phys* 15:075020
- Okada K, Yamamoto N, Kameshima Y, Yasumori A, Mackenzie KJD (2001) Effect of silica additive on the anatase-to-rutile phase transition. *J Am Chem Soc* 84:1591–1596
- Matteucci F, Cruciani G, Dondi M, Raimondo M (2006) The role of counterions (Mo, Nb, Sb, W) in Cr-, Mn-, Ni- and V-doped rutile ceramic pigments: part 1. Crystal structure and phase transformations. *Ceram Int* 32:385–392
- Choudhury B, Choudhury A (2012) Dopant induced changes in structural and optical properties of Cr^{3+} doped TiO_2 nanoparticles. *Mater Chem Phys* 132:1112–1118

18. Bonet A, Baben M, Travitzky N, Greil P (2016) High-temperature electrical conductivity of $\text{LaCr}_{1-x}\text{Co}_x\text{O}_3$ ceramics. *J Am Chem Soc* 99:917–921
19. Sang ML, HH L, Hong SC (2014) Influence of calcination temperature on Ce/TiO₂ catalysis of selective catalytic oxidation of NH₃ to N₂. *Appl Catal A Gen* 470:189–198
20. Wang H, Chen X, Gao S, Wu Z, Liu Y, Weng X (2013) Deactivation mechanism of Ce/TiO₂ selective catalytic reduction catalysts by the loading of sodium and calcium salts. *Catal Sci Technol* 3:715–722
21. Yang S, Zhu W, Jiang Z, Chen Z, Wang J (2006) The surface properties and the activities in catalytic wet air oxidation over CeO₂-TiO₂ catalysts. *Appl Surf Sci* 252:8499–8505
22. Huheey JE, Ellen AK, Richard L (1997) *Inorganic chemistry: principles of structure and reactivity*, 4th edn. Prentice Hall, New Jersey
23. Lopez-Navarrete E, Caballero A, Orera VM, Lázaro FJ, Ocaña M (2003) Oxidation state and localization of chromium ions in Cr-doped cassiterite and Cr-doped malayaite. *Acta Mater* 51:2371–2381
24. Lyubenova TS, Ocaña M, Carda J (2008) Brown ceramic pigments based on chromium(III)-doped titanite obtained by spray pyrolysis. *Dyes Pigments* 79:265–269

Submit your manuscript to a SpringerOpen[®] journal and benefit from:

- ▶ Convenient online submission
- ▶ Rigorous peer review
- ▶ Open access: articles freely available online
- ▶ High visibility within the field
- ▶ Retaining the copyright to your article

Submit your next manuscript at ▶ springeropen.com
